Water sources in semi-arid Northeast Asia as revealed by field observations and isotope transport model

[1]Tomonori Sato, [2]Maki Tsujimura, [2]Tsutomu Yamanaka, [3]Hiroyuki Iwasaki, [4]Atsuko Sugimoto, [2]Michiaki Sugita, [2]Fujio Kimura, [5]Gombo Davaa, [5]Dambaravjaa Oyunbaatar

[1] Japan Society for the Promotion of Science research fellow /
Center for climate system research, University of Tokyo, Kashiwa, Japan
[2] Graduate school of life and environmental sciences, University of Tsukuba, Tsukuba, Japan
[3] Faculty of Education, Gunma University, Maebashi, Japan
[4] Faculty of environmental earth science, Hokkaido University, Sapporo, Japan
[5] Institute of meteorology and hydrology, Ulaanbaatar, Mongolia

Submitted to *J. Geophys. Res. -Atmospheres-*
(Submitted December 8, 2006; Revised April 6, 2007)

Corresponding author
Tomonori Sato
Center for Climate System Research, University of Tokyo
5-1-5 Kashiwanoha, Kashiwa, 277-8568, Japan
Tel: +81-4-7136-4411, Fax: +81-4-7136-4375
E-mail: t_sato@ccsr.u-tokyo.ac.jp

Abstract

Origin of water vapor, which falls as precipitation over arid/semi-arid area in Northeast Asia, is investigated by modeling and observational approaches. The regional climate model evaluates the spatio-temporal variations of precipitation and water vapor budget, which are used to drive single-layer isotope circulation model. Intraseasonal variations of $\delta^{18}O$ in precipitation are well simulated during June-July-August of 2003. The $\delta^{18}O$ in water vapor experiences rapid decreases according to the passage of synoptic-scale disturbances. The rapid decreases of $\delta^{18}O$ are attributed to two processes. (1) The $\delta^{18}O$ in airmass locally decreases over the western mountains associated with the mountain precipitation; the light vapor is advected to eastern Mongolia by the prevailing westerly wind. (2) Convective systems pass by in the vicinity of the observation site, which persistently keep the lower $\delta^{18}O$ in the airmass.

Origin of the water vapor during June-July-August in 2003 is evaluated by the colored moisture analysis in which the tracers are assigned depending on the region where the water vapor finally evaporated. Seasonal mean result indicates that the regions contributing to precipitation in Mongolia are not low-latitude regions but Central Asia and Western Siberia located to northwest of Mongolia. Observed multi-level isotopic composition supports the model estimation. The moisture transport along the southwesterly wind of the Asian summer monsoon is difficult to reach Mongolia as monthly/seasonal mean perspective. However, eastern Mongolia and Northeast China are situated on the border area between westerly wind moisture transport, by middle-latitude synoptic cyclones, and southerly wind moisture transport, by Asian summer monsoon.

1. Introduction

The arid climate extends in Northeast Asia around North China and Mongolia while the major desert climate locates under the subtropical high zones corresponding to the subsidence branches of the Hadley circulation. Mongolia is situated in the northeastern part of the arid region. The precipitation is ranging from less than 50 mm $year^{-1}$ in the southern Gobi desert to more than 350 mm $year^{-1}$ in the northern Taiga forest, which should have the determinative influence on the vegetation cover in Mongolia as well as the mean temperature. Although the territory is located in the arid/semi-arid region, precipitation is supplied by the synoptic-scale disturbances during the warm season (June-July-August) because the country being in the westerly-dominant zone. However, due to the large interannual variation of precipitation, the climate change, which may be induced by the global warming, might give considerable impacts on the grazing activities, agricultural production, and consequently, economic production of the nation. Therefore, it is urgently demanded to investigate the interannual variability of the precipitation and its controlling mechanisms in this region. In recent years, this area has faced with a severe land degradation, whose concern is the feedback to regional climate system [Watson et al., 1998]. Xue [1996] suggested, from general circulation model (GCM) experiments, that the desertification alters the regional climate over Mongolia resulting in the rainfall reduction. Therefore, the land cover modification may also change the hydrological cycle through reduction of the evapotranspiration or the enhanced convective activity.

The origins of water vapor existing over Mongolia have been considered to consist of evapotranspiration at several regions such as Atlantic Ocean and tropical Asia [Yatagai and Yasunari,

1998; Numaguti, 1999]. Atmospheric water budget analysis can be a measure of the vapor origins in respect of understanding the local or remote contributions. Additionally, each component in the atmospheric moisture budget is deeply related to the rainfall variability that includes the extreme climate events like drought and flood [Yatagai and Yasunari, 1998]. Since the composition of the oxygen stable isotope in atmospheric moisture varies according to the phase change of the water, the isotope ratios in precipitation and water vapor are useful to examine the record of the water during transportation [e. g., Yamanaka et al., 2002]. During 2003, the intensive observation was conducted in eastern Mongolia under the RAISE (The Rangelands Atmosphere-Hydrosphere-Biosphere Interaction Study Experiment in Northeastern Asia) project [Sugita et al., 2007]. Water samples collected from precipitation, near-surface vapor, and vapor in the free atmosphere were analyzed to investigate the isotopic composition. Yamanaka et al. [2007] revealed, using the observed isotope data, that the $\delta^{18}O$ in precipitation shows large seasonal variation which is almost corresponding to the seasonal cycle of air temperature. They further clarified that the intraseasonal variation of the $\delta^{18}O$ in precipitation can be predictable as a function of temperature and precipitation at the observation site. However, the spatial distribution of $\delta^{18}O$ and the origins of water vapor have not been clarified so far.

Climate models which incorporates the isotope processes makes us possible to diagnose water cycle in respect of both isotopic variation and water origins [e.g., Bosilovich and Schubert, 2002; Koster et al., 1986; Numaguti, 1999]. Additionally, isotopic variations in a wider area, i.e. global-scale or continental-scale, are able to be discussed using the model while the observational data provides us only on-site but valuable information. Isotopic characteristics in water vapor and

precipitation may be capable of applying to researches on future changes of atmospheric circulation under the global warming and the desertification, both of which are the real threats recently in the study area. For example, changes of the atmospheric circulation and the land-atmosphere interaction affect the stable isotope composition in a certain area according to the changes in water origins or transportation routes. The GCMs have advantage to study longer-term variations or global distributions of isotopic composition. However, the rainfall distribution is very complicated in the study area, mainly due to the complex topography in and around Mongolia. Therefore, the prerequisite for the climate model is to resolve the interaction between the topography and convective systems. The regional climate model presented by Sato et al. [2007] performed a good simulation of rainfall in July over Mongolia, in which the meridional gradient of precipitation, as addressed earlier, was well reproduced.

Integration of such a unique and high quality isotope observations during RAISE will be a great aid for developing a conceptual model of water sources in semi-arid area. In this study, we develop an isotope transport model which is driven by the regional climate model, the results from which are firstly compared with the observed isotopic values. The objectives of this study are, (1) to clarify the mechanism for the observed intraseasonal variation of the $\delta^{18}O$ in precipitation in relation to the spatial structure of the isotopic composition around Mongolia, (2) to evaluate the sources of precipitable water in Mongolia, using a newly developed model. Atmospheric water budget analysis is conducted in Section 2. In Section 3, we describe the application of a single-layer Rayleigh-type isotope circulation model to the use in regional climate model. Spatio-temporal variation of $\delta^{18}O$ is described in Section 4. Discussions on water vapor origins of Mongolian precipitation are addressed

in Section 5. Limitation and applicability of the model are summarized in Section 6.

2. Atmospheric water balance

As mentioned in Section 1, each component of the atmospheric water budget is useful to describe the climate mean field of the moisture transport in the study area [e.g., Yatagai, 2003]. Here, 6-hourly National Centers for Environmental Prediction (NCEP)/ National Center for Atmospheric Research (NCAR) reanalysis data [Kalnay et al., 1996] is used to compute the moisture advection around Mongolia. Water vapor flux around Mongolia is computed in the same method to that shown in Oki et al. [1995] using wind speed, temperature, relative humidity, and surface pressure from the reanalysis data. The long-term mean of rainfall is calculated using the CPC (Climate Prediction Center) Merged Analysis of Precipitation (CMAP; Xie and Arkin, 1997). Calculations are carried out for 25 years from 1979 through 2003.

Figure 1 shows the amount of atmospheric water vapor flux around Mongolia during June, July and August. The values in the parentheses indicate the standard deviations during 25 years. The convergence of atmospheric moisture becomes close to zero during June-July-August. As a result, the evapotranspiration, as simply evaluated by precipitation minus convergence, is comparable to the precipitation, which denotes that the moisture from local evapotranspiration contributes significantly to the precipitation in Mongolia. Additionally, from the GCMs simulations, this region is known as a high recycling ratio among the world [Bosilovich and Schubert, 2002]. However, notice has to be paid that, although the convergence is negligibly small in the water budget, huge amount of moisture

is continuously transported through Mongolia. The principal route of moisture transport is zonal direction which is several times larger than the meridional transport. The incoming moisture from the western boundary is the largest among four components, and is more stable with small interannual variability. On the other hand, meridional moisture transport has larger standard deviation than that of 25-year mean. Therefore, the direction of meridional moisture transport varies depending on the year as indicated by Yatagai [2003].

The inspection of the atmospheric water vapor budget implies relatively small contribution of the local evapotranspiration in Mongolia. According to the simple estimation [Brubaker, 1993], the ratio of locally evaporated to total precipitation (R) is defined as

$$R = \frac{EL}{EL + 2F_{in}}$$

, where E is the evapotranspiration, L is the length of domain considered, and F_{in} is the moisture flux into the domain. Trenberth [1999] showed that the R is smaller than 10 % around eastern Mongolia during June-July-August. These facts indicate that most part of water vapor is originated to the west rather than that originated to the south of Mongolia albeit the moisture transport along the Asian summer monsoon seems to have some contributions in this region in relation to the extension of the Asian summer monsoon. Quantitative evaluation of water sources are examined using the numerical model in Section 5 after the description and the validation of the model in Section 3 and 4.

3. Model description

In section 2 we briefly analyzed the climatological mean state of the atmospheric water budget using the reanalysis data. In order to evaluate water budget and water origins as a comparable form with the isotope observation, a single-layer isotope circulation model is developed into the Terrestrial Environmental Research Center - Regional Atmospheric Modeling System (TERC-RAMS; Sato and Kimura, 2005). Configurations and detail settings of the model for the calculation of the atmospheric circulation including the precipitation systems around Mongolia are described in Sato et al. [2007]. The calculation domain covers 12,000 km x 9,000 km range centered on the Tibetan Plateau (See also Figure 11) with 150 km horizontal resolution. Two-way nesting grid system is adopted covering Mongolian territory with 30 km resolution, which enhances the model accuracy for moisture transport even in the 150 km resolution grid system. In this study, 150 km resolution grid variables are used for isotope simulation in order to cover as large area as possible which potentially relates to the hydrological cycle in Mongolia. Although the resolution is not high, nested isotope simulation with 30 km resolution conducted very similar results to that presented in this study. The model atmosphere is nudged to the NCEP/NCAR reanalysis data. Surface conditions in the TERC-RAMS domains are given by a global land cover characterization dataset provided by the U. S. geological survey [Loveland et al., 2000]. Detail evaluation of the rainfall reproducibility appears in Sato et al. [2007]. Soil parameterization in the TERC-RAMS is presented by Tremback and Kessler [1985], which involves prognostic equations for soil surface temperature and water content. For the vegetation cover, the TERC-RAMS uses distributions of the Leaf Area Index (LAI), the vegetation albedo, the roughness height, and other parameters of vegetation determined in the Biosphere–Atmosphere Transfer Scheme (BATS; Dickinson et al., 1986). The initial soil moisture at the eleven soil layers is obtained by one month spin-up integration. The surface sensible and latent

fluxes calculated by Louis [1979] are compared with the observations measured by the eddy-covariance method in Mongolia [Sato and Kimura, 2006].

Figure 3 shows time series of precipitable water vapor (PWV) at eastern Mongolia during June, July, and August of 2003. Dots indicate the PWV variation obtained by GPS (Global Positioning System) sounding at Kherlen-Bayan-Ulaan (KBU; 108.78^{o}E, 47.28^{o}N, 1250 m). Detail explanations of the GPS observation were addressed by Iwasaki et al. [2007]. The TERC-RAMS provides a quite similar PWV variation with the observed one, in which the correlation coefficient is 0.72 for the hourly interval comparison. The PWVs from model and reanalysis data are relatively smooth while GPS-derived PWV shows pronounced peaks in the temporal variation because the area-averaged values are shown by the model and reanalysis data. In order to carry out the isotope transport simulation, moisture transport and precipitation are demanded with high accuracy as discussed in Yoshimura et al. [2003]. These two prerequisites are achieved by the TERC-RAMS, which is the advantage to conduct isotope simulation in this area with regional climate model.

Oxygen stable isotope transport process in the atmosphere is computed by the Isotope Circulation Model (ICM) which was presented by Yoshimura et al. [2003]. The ICM is based on a single-layer moisture transport model. At each time step, water budget and isotope budget before considering precipitation are firstly computed for the column atmosphere using the hourly variables from regional climate model. Secondly, the Rayleigh isotopic fractionation is considered depending on the amount of precipitation in each grid box. The ICM assumes that the evapotranspired moisture is immediately mixed with environmental atmosphere in a column, the validity of which was

examined in Yoshimura et al. [2003] for tropical Asia. Since current study applies this assumption to the middle-latitude semi-arid area, we discuss the ability of the ICM in the latter section. The lateral boundary condition of the oxygen stable isotope in water vapor is,

$$\frac{\partial\left(\delta^{18}\mathrm{O}\right)}{\partial x} = 0 \quad \text{at the west and east boundaries}$$

$$\frac{\partial\left(\delta^{18}\mathrm{O}\right)}{\partial y} = 0 \quad \text{at the south and north boundaries}$$

Therefore, the isotopic composition at outside of the boundary is assumed to have the same value to that at the boundary grids. The $\delta^{18}O$ in the evapotranspired vapor is determined by a function of the latitude and altitude based on the estimation of Bowen and Wilkinson [2002]. The $\delta^{18}O$ in the vapor initially existing in the atmosphere is also assumed by their estimation. Evaporated water from the ocean including the Black Sea and the Caspian Sea has a constant $\delta^{18}O$ with -9.6 ‰ which may be too light when kinetic fractionation is considered [Yoshimura et al., 2006]. Discussions on the isotope fluxes from the surface and the lateral boundaries are appeared in Section 6.1. Temperature at 700 hPa level is used to determine the equilibrium fractionation factor based on the equation by Majoube [1970]. Simulation for the isotopic variation is carried out from 28th May 2003 to the end of August 2003 corresponding to the RAISE intensive observing period (May-November 2003). Although the TERC-RAMS adopts the cumulus parameterization [Arakawa and Schubert, 1974] and Microphysics parameterization [Walko et al., 1995], isotopic fractionation in the convective system is not explicitly calculated in the ICM.

4. Simulated $\delta^{18}O$ variation

This section firstly compares the simulated isotope variation with the observed values during the

RAISE intensive observation in 2003. Using the results from the ICM, mechanism of the isotopic composition and its spatial distributions are described in this section.

4.1 Observations and simulated $\delta^{18}O$

As described in Section 1, the intensive observation was conducted at eastern Mongolia in 2003. Precipitating water samples were collected at seven sites in Mongolia with daily interval, and isotopic composition of oxygen stable isotope (^{18}O) was analyzed. Detailed descriptions on the observing systems appeared in Yamanaka et al. [2007]. This study uses the five stations which locate in eastern Mongolia and have continuous observations throughout June through August. Aircraft measurements were carried out on 19th, 20th, 23rd July, and 21st, 22nd, 23rd August to collect the water vapor in the upper-air. We use $\delta^{18}O$ from aircraft observations to compare with the modeled values. Atmospheric water vapor near ground surface was also sampled in four terms of 2003, 8th to 19th June, 18th to 24th July, 18th to 23rd August, and 29th September to 4th October, at the KBU site and the Forest site (108.65^{o}E, 48.35^{o}N, 1632 m). Multi-level measurements of isotopic composition make us possible to distinguish between the evapotranspired moisture and the advected moisture, which will be a valuable observation-based evidence for the validation of moisture sources given by the model in Section 5. The water collection systems and the observed isotopic features were summarized in Tsujimura et al. [2007].

Scatter plot of the isotopic composition between the observations and their nearest grid points in the ICM are shown in Figure 4. Correlation coefficients at Mongenmorit (108.50^{o}E, 48.20^{o}N) and

Mandalgobi (106.27°E, 45.75°N) are 0.48 and 0.54, respectively. On the other hand, the correlation at Ulaanbaatar (106.87°E, 47.92°N) is rather low. The reason may come from the lack of model resolution. Figure 5 illustrates the time series of $\delta^{18}O$ in precipitation and water vapor. The ICM results are shown by the spatially averaged values covering some of the observation sites because the number of the observed rainfall samples is not enough to compare the ICM and the observation at each site owing to the characteristics of the precipitation systems in the semi-arid area, i.e., short-term and small-scale. The ICM well replicates the observed intraseasonal variation of $\delta^{18}O$ in precipitation, which oscillates with a few-day interval. The model succeeds in simulating the events in which the $\delta^{18}O$ experiences a drastic drop (e.g., in 28th June, 19th July, and 15th August). In these cases, simulated $\delta^{18}O$ agrees well to the observed values in temporal and amplitude of the changes. As compared with Figure 3, these drops in $\delta^{18}O$ occur simultaneously with the sudden PWV decreases, which indicate that the intraseasonal variation of isotopic composition is strongly affected by the synoptic-scale atmospheric circulations. Generally, a sudden decrease of PWV is known to occur when the cold air mass is advected following the cold front [Okamura and Kimura, 2003]. On the other hand, the model tends to underestimate the high-$\delta^{18}O$ cases observed at Ulaanbaatar around 30th June and 14th July. In these cases, observed value at each station distribute approximately in 10 ‰ range in the both days, e.g., 1.32 ‰ at Ulaanbaatar, -8.64 ‰ at Mongenmorit, and -9.12 ‰ at Mandalgobi in 14th July. The 150 km-resolution model cannot resolve the subgrid information of $\delta^{18}O$ since the ICM represents the spatially averaged isotopic composition in 150 x 150 km grid box. Additionally, the observed isotopic composition can be a result of evaporation of rain water below the cloud base that is likely to cause such high $\delta^{18}O$ values [Yamanaka et al., 2007]. The evaporation of rain drops occurs more efficiently when the daytime mixed layer is drier in the semi-arid area.

Therefore, short-term precipitation associated with the diurnal cycle around the mountain may be more sensitive to the evaporation under the clouds rather than the longer term precipitation event associated with the synoptic-scale disturbances.

During the RAISE intensive observing period, $\delta^{18}O$ in water vapor was measured by aircraft observations [Tsujimura et al., 2007]. In 20th July, simulated $\delta^{18}O$ in vapor agrees well to the observation. In other cases, however, the model tends to overestimate $\delta^{18}O$. The limitations of the ICM used in this study, i.e., constant $\delta^{18}O$ value from evapotranspiration, lateral boundary, and single-layer description are attributed to the inconsistency between the ICM and the observations, which are discussed in Section 6.1. During the three cases in June, single-layer assumption seems not to affect the overestimation since vertical profile of the observed $\delta^{18}O$ was almost constant [Figure 5 and Tsujimura et al., 2007]. The isotope model reproduces the decreasing trend in 23rd July although the time lag and spatial inconsistencies are recognized. On the other hand, during three observations in August, $\delta^{18}O$ declined with altitude around the lower troposphere, and heterogeneously distributed over eastern Mongolia [Tsujimura et al., 2007]. Additionally, drastic decreases of the $\delta^{18}O$ occurred after 21st August in all levels. The ICM fails to reproduce this phenomenon. Nevertheless, as in the Figure 3, the TERC-RAMS succeeds in simulating a sudden PWV decrease in 22nd August. Furthermore, the simulated $\delta^{18}O$ in precipitation shows a drop corresponding to the observed event. The sudden drop of $\delta^{18}O$ in vapor is detected over east of Lake Baikal as shown by the broken line in Figure 5. From these facts, the failure of the drastic change of $\delta^{18}O$ in vapor in August cases can be attributed to the isotope process, in particular, the single-layer treatment in the ICM rather than the atmospheric circulation simulated by the TERC-RAMS..

4.2 Processes controlling the $\delta^{18}O$ variation

Figure 6 shows Hovmoller diagram of the simulated $\delta^{18}O$ in water vapor over Mongolia along 80-130^{o}E. In all cases when $\delta^{18}O$ experiences the sudden drop in observation site, the airmass which contains light vapor is transported from the western Mongolia. The light vapor is originally generated around the mountain range to the east. The spatio-temporal variation of the $\delta^{18}O$ is very similar to that of precipitation (no figures). The generation of the light vapor in the mountain area is associated with the initialization of the convective systems because the complex terrain over western Mongolia is very important to generate the precipitation systems [Sato, 2005].

In order to examine the spatial characteristics of the vapor $\delta^{18}O$ variation, time series of rainfall distribution and $\delta^{18}O$ in the water vapor are shown in Figure 7. In 23rd June, precipitation occurs around the Altai Mountains (88^{o}E, 50^{o}N) due to the cold trough. Although, at the 00Z 23rd, the $\delta^{18}O$ around the mountain does not prominently low, it rapidly decreased forming a local minimum with -28 ‰ after 12 hours. The precipitation system moves eastward; and, the area of minimum $\delta^{18}O$ also propagates to eastern Mongolia. The center of the light vapor airmass passes by the observation site around 27th June, which causes the drastic drop of the $\delta^{18}O$ in collected precipitation.

In the ICM, we can quantitatively separate the contribution of each process on $\delta^{18}O$ variation, such as precipitation, advection, and evaporation, which act to change the isotopic composition. Figure 8 shows the time series of $\delta^{18}O$ budget around the observation site. The $\delta^{18}O$ continuously

decreases from 00Z 24th June through 08Z 27th June. Tendency of $\delta^{18}O$ almost follows the advection term before 12Z 25th June, which indicates that the decrease of $\delta^{18}O$ is mainly caused by the advection process; in other words, light vapor advects over the observation site. After that, the advection term tends to show positive value indicating heavy vapor advection. Meanwhile, $\delta^{18}O$ continues to decrease owing to local precipitation which is, in turn, a dominant factor controlling $\delta^{18}O$ variation. Therefore, both the advection of moisture and the precipitation near observation site plays key role to decrease the $\delta^{18}O$ in the water vapor in this event.

Another typical case with $\delta^{18}O$ drop occurs in 11th to 16th August as shown in Figure 9. In this case, precipitation occurs west of the Lake Baikal, around 111^{o}E 53^{o}N, before 00Z 12th August. In 00Z 13th August, the model simulates the decrease of $\delta^{18}O$ and light center of $\delta^{18}O$ in water vapor. The precipitation system stayed around the Lake Baikal before 00Z 14th August. Therefore, the area with low $\delta^{18}O$ airmass diffused in the central Mongolia. After 00Z 15th August, precipitation system exhibits an anticlockwise circulation indicating a development of the cyclone. The advection of the light airmass is reaching to the eastern Mongolia, which consequently decreases the $\delta^{18}O$ even where the precipitation does not occur. Throughout this event, temporal variation of $\delta^{18}O$ is almost controlled by the advection term only (Figure 10); and, the contributions of precipitation and evaporation are negligibly small.

In these cases, the drastic decrease of the $\delta^{18}O$ in eastern Mongolia can be governed by the two processes, the advection and the precipitation (Rayleigh) process. In the August case, as shown in Figure 10, advection of the light vapor, which is generated around the mountain due to the Rayleigh

process, mostly contributes to the drastic decrease of $\delta^{18}O$ at the observation site. This is because the $\delta^{18}O$ variation is observed even without precipitation around the observation site in the model. On the other hand, in the late June case (Figure 8), both processes are deeply related to the decrease of $\delta^{18}O$. During the first stage from 24th to 25th June, the advection of the light vapor decreases the $\delta^{18}O$ in the observation site. Meanwhile, in the second stage from 26th to 28th June, advection term increases the $\delta^{18}O$. At the same time, the Rayleigh process tends to decrease the column averaged $\delta^{18}O$. The decrease due to the precipitation overcomes the increase due to advection process in the second stage; thus, the $\delta^{18}O$ continuously decreases during these two stages in the June case. Since the low $\delta^{18}O$ appears corresponding to the PWV decrease, the low $\delta^{18}O$ indicates the cold air advection after the passage of synoptic-scale disturbances. This is because the intraseasonal variation of $\delta^{18}O$ can be excellently explained by the temperature variation as in Yamanaka et al. [2007].

In this section, the ability of the ICM in regional climate model is examined. The model reproduces the characteristic intraseasonal variation of isotopic composition which is mainly controlled by the advection and the precipitation processes. The well-mixed assumption in the isotope processes seems to be valid in both of these cases. In the next section, we evaluate the moisture sources in Northeast Asia based on the same modeling framework.

5. Origin of water vapor in semi-arid Northeast Asia

Many studies that aimed at estimating the water origins in certain areas have been carried out previously, mainly using the GCMs [Bosilovich and Schubert, 2002; Koster et al., 1986; Numaguti,

1999]. Yoshimura et al. [2004] developed the Colored Moisture Analysis (CMA) technique to study water sources in Asian monsoon region, in which the reanalysis data is used for the computation of the atmospheric water budget because the source determination can be strongly affected by the large-scale atmospheric circulation in which the GCMs may have biases. In this study, the regional climate model is used to implement the CMA and to determine the sources of water in Mongolia as in the same reasons to adopt it for the isotope simulation. High performance of water vapor budget in the regional climate model, which has been proved by the isotope simulation, is expected as a benefit to use it for moisture source estimation.

The atmospheric water budget component in the ICM, which is addressed in Section 2, is modified in order to utilize it for the estimation of the water vapor sources. The number of tracer is increased up to sixteen, and the concentration of each tracer is computed using the amount of hourly evapotranspiration at each region as appeared in Figure 11. Since the TERC-RAMS has the lateral boundaries, tracers are also assigned for the four (EWSN) boundaries in order to examine the contributions of the water vapor penetrating the boundaries. The concentrations of the boundary tracers are determined by the water vapor flux across the boundaries, which is evaluated using the TERC-RAMS simulation. It is assumed, in the CMA, concentration of each tracer is identical between rain water and the atmosphere in the precipitating column.

Figure 12 shows the intraseasonal variation of the water vapor sources over eastern Mongolia. The colored areas represent the contribution ratio of the evapotranspiration from the defined regions to the total PWV at eastern Mongolia. The total of all region's contributions exactly coincide to the

PWV. Black colored area means the water vapor initially existed in the model domain, which rapidly attenuated by the evapotranspiration and moisture transportation from the outside of the model domain. Colors below the white line indicate the water vapor penetrated through the lateral boundaries. Because the TERC-RAMS adopts a polar-stereographic projection, the direction of the upper boundary in Figure 11 is not always north but contains northwest and northeast (See Figure 11). The water vapor in eastern Mongolia is mainly originated by the Central Asia, Siberia, and Mongolia. When the peak of PWV occurs, corresponding to the passage of precipitation systems, water vapor evaporated at Central Asia prominently increases its amount. Thus, synoptic-scale disturbances, like cyclones and front systems, transport huge amount of water vapor from the western regions. On the other hand, water vapor evaporated at low-latitude regions, such as Pacific Ocean, Indochina Peninsula, and Indian Ocean, contributes very little in eastern Mongolia compared to the middle- and high-latitude origins. Intrusion of low-latitude-originated water vapor can be detected from 8th to 20th July. However, other regions are increasing their contribution ratios at the same time. In case from 1st to 5th August, only tropical origins become large while the other origins are kept small, which indicates the water transport from the south enhances the PWV in this period. It has been known that monsoon flow along the eastern coast of the Eurasian continent transports huge amount of water vapor at least up to northern China around 45^{o}N [Ding, 1994]. The CMA revealed that the main sources of water vapor are not originated to the south but to the west, and most part of water vapor is transported by the synoptic disturbances and the ambient westerly wind. Although our evaluations are based on the June-July-August in 1998, the results can be regarded as an index of the atmospheric circulation which will be useful to investigate the interannual variations, land cover change, and the global-scale climate change.

Figure 13 shows the composition of water vapor origins at Inner Mongolia, China (110-115^{o}E, 40-45^{o}N). Contrastingly to the Mongolian case in Figure 12, various origins are compounded in this area. Water vapor from Mongolia, Central Asia, eastern China, and tropical regions are comparably existed. During middle July, more than half portion of the water vapor is coming from low-latitude Asia and tropical oceans. Therefore, water vapor transportation along the monsoon flow largely contributes to the water vapor composition in Inner Mongolia as well as that maintained by the synoptic-scale disturbances.

In eastern Mongolia, the contribution of tropical water vapor is less than 10 % in June-July-August average. However, the large gradient exists around Inner Mongolia between Mongolia and Northeast China. Therefore, the contribution of tropical-originated water drastically increases to the southeastward. In Inner Mongolia, it reaches 20-40 %. The eastern Mongolia and Northeast China is indeed situated on the border area between westerly wind (middle-latitude synoptic cyclones) originated moisture and southerly wind (monsoon) originated moisture.

In general, it has been difficult, so far, to validate the simulated sources quantitatively based on the observed evidence. The Keeling plot analysis [Yakir and Sternberg, 2000] is applied to evaluate the contribution ratio of local evapotranspiration to the total amount of water vapor in the atmospheric boundary layer using multi-layer observations of $\delta^{18}O$ in vapor. Tsujimura et al. [2007] found that the contribution ratio of local evapotranspiration could be 30-46 % at the Forest site on 23rd August and 25-44 % at the KBU site on 21st August. Although the distinct separation between

1 the Forest and the KBU site seems to be difficult with 150 km resolution, the CMA estimates
2 approximately 25-40 % of the PWV in eastern Mongolia as a local evapotranspiration during 21st to
3 23rd August (See Figure 12). One has to note that there are some assumptions both in the
4 Keeling-plot analysis and in the model. In the CMA, the word "local" exactly corresponds to the area
5 with red color in the Figure 11 while, in the Keeling-plot, it will be more ambiguous and be
6 applicable to the area where $\delta^{18}O$ in evapotranspired vapor exhibits a similar value. Although, thus,
7 the accurate contribution ratio still need to be examined in the future study, the robust fact from these
8 two approaches is that the evapotranspiration in Mongolia does not only primal contributor to the
9 atmospheric water vapor in Mongolia. As in the Section 2, the evapotranspiration become
10 comparable to the precipitation, and atmospheric convergence become close to zero in the
11 June-July-August average. Nevertheless, the amount of water vapor passing through Mongolia is
12 very large which should not be negligible; thus, in actual, the evapotranspired water in Mongolia is
13 well-mixed with advected vapor and is comprised in the zonal moisture transport.
14
15
16 **6. Discussion**
17 6.1 Validity to use ICM with regional climate model
18 This section mainly discusses on the validity to use the ICM with the regional climate model,
19 which contains assumptions for simplicity. In this study, $\delta^{18}O$ from land evapotranspiration is very
20 simply given without varying in time. Mongolia is apart from the oceans, and locates in the eastern
21 flank of the Eurasian continent where most part of precipitation is a result of the recycling over land
22 [Bosilovich and Schubert, 2002; Numaguti, 1999]. Therefore, $\delta^{18}O$ in the evapotranspired water

should be lower than that defined in the model as a function of the latitude and the altitude. The uniform value of the $\delta^{18}O$ in evaporation from water bodies is also one of the simplifications in our model. According to Yoshimura et al. [2006], -9.6 ‰ for evaporated water will be too light when kinetic fractionation is considered. Fortunately, as shown in Fig. 11, water vapor evaporated at low-latitude ocean has little impact on the water budget in eastern Mongolia, whereas evaporation from the Black sea and the Caspian Sea may induce slightly higher values in the study area. There are lateral boundaries in the TERC-RAMS, which may reduce the model accuracy to simulate the $\delta^{18}O$ variation in case that incoming vapor flux is large through the boundaries. On the other hand, the purpose of this study is to simulate and to investigate the intraseasonal variation of the $\delta^{18}O$. For this purpose, the regional climate model has advantage in accurately simulating the temporal variation of water vapor transport associated with synoptic disturbances. Thus, our results can be applicable to intraseasonal variability although there is continuous bias causing lower $\delta^{18}O$ of water vapor due to the reasons mentioned above. Additionally, evaporation of rain drops may have large influence on the $\delta^{18}O$ over the arid/semi-arid regions. Unfortunately, the number of water vapor samples in free atmosphere is not sufficient to investigate the influence of evaporation below cloud base. The influence of cloud base evaporation of the rain drops can be larger when the daytime mixed layer is drier. Over eastern Mongolia, short-term but sometimes heavy precipitation tends to occur during daytime in association with the diurnal cycle of the atmosphere. In these cases post condensation process should be considered.

This study applies a single-layer isotope transport model to the middle-latitude arid/semi-arid region. The model was coordinated on the basis of well-mixed assumption, in which the

evapotranspired water is immediately mixed with an environmental atmosphere in a column [Yoshimura et al., 2003]. One may think that the assumption is not suitable for describing the middle-latitude climate. However, the amount of the water vapor is strongly dependent on the altitude concentrating in the lower troposphere. Hence, the movement of the water vapor ought to follow the lower tropospheric wind which is strongly affected by the topography. The regional climate model used in this study captures the major mountain area in Mongolia, which leads to the well replication of the $\delta^{18}O$ variation albeit a single-layer simplification in the Rayleigh-type ICM. On the other hand, the model failed to simulate the sudden drop of the $\delta^{18}O$ in 23rd August which was observed by the aircraft sounding although, in the model, the air mass with light vapor appears near the Lake Baikal instead of eastern Mongolia (broken line in Figure 4). There will be two causes that induce the failure, simulation of the atmospheric circulation and the assumptions in the ICM. The latter seems to be a cause for this case since the TERC-RAMS successfully simulated the sudden PWV drop in correspondence with this event. During this event, there was approximately 5 ‰ difference in $\delta^{18}O$ between near surface vapor and that above atmospheric boundary layer [Figure 5 and Tsujimura et al., 2007]. The single-layer model has a difficulty to simulate $\delta^{18}O$ variation in a case with large vertical gradient of $\delta^{18}O$ in a lower troposphere. Additionally, vertical shear exists in the wind direction; southerly wind prevails near surface while northerly wind around 700 hPa. Thus, the differential advection of moisture reduces the reproducibility of isotopic composition. The model has to be improved to simulate the vertical transport of isotopes. In the ICM, generally, the wind shear tends to cause large errors when (1) low-level wind and integrated moisture flux are in different direction, and (2) the isotopic composition is highly dependent on the altitude. In the latter case, however, the vertical profile of $\delta^{18}O$ is very difficult to observe without aircraft

sounding. The both conditions are conformed in 23rd August event; therefore, the single-layer description in the ICM seems to exceed a limit to describe the isotope circulation.

6.2 Relation between water origins and climate change

This study revealed that there is a border of water origins around the Northeast China. Water vapor advected along the Eurasian continent is dominant in Northeast Asia, which is also a result of the precipitation recycling. Another major water origin is the low-latitude Asia and the tropical oceans, the water from which is transported by the Asian summer monsoon circulation. These two components are mixed around the Northeast China causing the characteristic distribution of the water origins. Such drastic variations of water source component should also be evident in the stable isotope in precipitating water. Thus, the isotope observations in precipitation or lake sediments in this boundary area will provide valuable information on the Asian monsoon and mid-latitude storm activities in daily to millennium timescales. For example, global warming due to increasing greenhouse gas concentration may modify the Asian monsoon [Min et al., 2004; Kitoh et al., 1997: Kimoto, 2005] and also the storm track along the Eurasian continent [Ulbrich and Christoph, 1999]. The regional climate change, which is induced by the large-scale atmospheric circulations, could be detectable as a variation of water origins. In eastern Mongolia, contribution of the tropical origins tends to increase in the summer when the Asian monsoon is stronger and the moisture flow is penetrating further north. Therefore, longer-term variation of the water origins in this border area can be a proxy of the climate change in Northeast Asia.

The land cover / land use change may also influence the water origins in Northeast Asia. Xue [1996] suggested that the precipitation over the Mongolia is decreased after the grassland is replaced by the desert in the GCM. The regional climate model used in this study has already been applied to study these topics as in Sato and Kimura [2007]. They summarized that the precipitation tends to change more complicatedly having an interaction between the land surface process and the synoptic-scale disturbances. The reduction of the latent heat flux due to the land surface change can be apparent as the reduced contribution of the local evapotranspiration rather than the change of PWV. Thus, the CMA method will be a good tool for environmental study over the arid/semi-arid area in Northeast Asia, and the isotope observations are the most important way to validate the CMA results through checking the water budget component in the ICM. Further studies on the interannual and longer-term changes of water origins are necessary in relation to the interannual variation of precipitation in the arid/semi-arid region.

7. Conclusion

The origin of water vapor, which falls as precipitation over arid/semi-arid area of Mongolia, is investigated by the numerical experiment and the observed isotope data. The regional climate model evaluates the spatio-temporal variations of precipitation and water vapor budget in the area, which are used to drive the ICM. Intraseasonal variations of $\delta^{18}O$ in precipitation are well simulated during the period of June-July-August in 2003. The $\delta^{18}O$ in water vapor experiences rapid decreases as the synoptic-scale disturbances pass by the observation site. The rapid decrease of $\delta^{18}O$ is attributed to the following two processes. (1) The $\delta^{18}O$ in airmass locally decreases over the Altai and the Sayan

mountain areas associated with the mountain precipitation; the light vapor is advected to eastern Mongolia by the prevailing westerly wind. (2) Convective systems pass by in the vicinity of the observation site, which persistently keep the lower $\delta^{18}O$ in the airmass.

Origin of the water vapor is evaluated by the CMA in which the tracers are assigned depending on the region where the water vapor finally evaporated, and the concentrations of the tracers are determined by the amount of evapotranspiration. In the summer seasonal average in 2003, the regions which contribute to the precipitation in Mongolia are not low-latitude regions but Central Asia and Western Siberia located to the northwest of Mongolia. The moisture transport along the southwesterly wind of the Asian summer monsoon is difficult to reach Mongolia as a monthly/seasonal mean perspective during the summer of 2003. However, eastern Mongolia and Northeast China are situated on the border area between the westerly wind moisture transport, by middle-latitude synoptic cyclones, and southerly wind moisture transport, by the Asian summer monsoon. Simulated contribution ratio of local evapotranspiration to the total moisture is approximately 25-40 % during 21st to 23rd August. The estimation based on the multi-layer isotope observation was 30-46 % at the Forest site on 23rd August and 25-44 % at the KBU site on 21st August [Tsujimura et al., 2007]. Therefore, the both observational and modeling estimations are in good agreement in respect with that the local evapotranspiration is not an only source of moisture in Mongolia.

Acknowledgements

Constructive comments and suggestions by the anonymous reviewer's are greatly appreciated. This study was carried out under a RAISE project (Rangelands Atmosphere- hydrosphere-biosphere Interaction Study Experiment in Northeastern Asia) funded by CREST (Core Research for Evolutional Science and Technology) program of JST (Japan Science and Technology Agency). One of the authors (T.S) is supported by Japan Society for the Promotion of Science (JSPS) as a research fellow.

References

Arakawa, A., and W. H. Schubert (1974), Interaction of a cumulus cloud ensemble with the large-scale environment, Part I, *J. Atmos. Sci.*, **31**, 674–701.

Bosilovich, M. G., and S. D. Schubert (2002), Water vapor tracers as diagnostics of the regional hydrologic cycles, *J. Hydrometeor.*, **3**, 149-165.

Bowen, G. J., and B. Wilkinson (2002), Spatial distribution of $\delta^{18}O$ in meteoric precipitation, *Geology*, **30**, 315-318.

Brubaker, K. L., D. Entekhabi, and P. S. Eagleson (1993), Estimation of continental precipitation recycling, *J. Climate*, **6**, 1077-1089.

Dickinson, R. E., A. Henderson-Sellers, P. J. Kennedy, and M. F. Wilson (1986), Biosphere atmosphere transfer scheme (BATS) for the NCAR community climate model, *NCAR Technical Note NCAR/TN275+STR*, 69p.

Ding, Y. (1994), *Monsoons over China.* Kluwer Academic Publishers.

Iwasaki, H., T. Sato, T. Nii, F. Kimura, K. Nakagawa, I. Kaihotsu, and T. Koike (2007), Diurnal variation of convective activity and precipitable water around Ulaanbaator, Mongolia and impact of soil moisture on convective activity in the nighttime, Submitted to *Mon. Wea. Rev.*

Kalnay, E., M. Kanamitsu, R. Kistler, W. Collins, D. Deaven, L. Gandin, M. Iredell, S. Saha, G. White, J. Woollen, Y. Zhu, A. Leetmaa, B. Reynolds, M. Chelliah, W. Ebisuzaki, W. Higgins, J. Janowiak, K. C. Mo, C. Ropelewski, J. Wang, R. Jenne, and D. Joseph (1996), The NCEP/NCAR 40-Year Reanalysis Project, *Bull. Amer. Meteor. Soc.*, **77**, 437-471.

Kimoto, M. (2005), Simulated change of the east Asian circulation under global warming scenario, *Geophys. Res. Lett.*, **32**, L16701, doi:10.1029/2005GL023383.

Kitoh, A., S. Yukimoto, A. Noda, and T. Motoi (1997), Simulated changes in the Asian summer monsoon at times of increased atmospheric CO_2, *J. Meteor. Soc. Japan*, **75**, 1019-1031.

Koster, R. D., J. Jouzel, R. J. Suozzo, G. L. Russell, W. S. Broecker, D. Rind, and P. S. Eagleson (1986), Global sources of local precipitation as determined by the NASA/GISS GCM, *Geophys. Res. Lett.*, **13**, 121-124.

Louis, J.-F. (1979), A parametric model of vertical eddy fluxes in the atmosphere, *Bound.-Layer Meteor.*, **17**, 187–202.

Loveland, T. R., B. C. Reed, J. F. Brown, D. O. Ohlen, J. Zhu, L. Yang, and J. W. Merchant (2000), Development of a global land cover characteristics database and IGBP DISC over from 1-km AVHRR data, *Int. J. Remote Sens.*, **21**, 1303-1330.

Majoube, M. (1971), Fractionnement en oxygen-18 et en deuterium entre leau et sa vapeur, *J. Chem. Phys.*, **68**, 1423-1436.

Min, S.-K., E.-H. Park, and W.-T. Kwon (2004), Future projections of East Asian climate change from multi-AOGCM ensembles of IPCC SRES scenario simulations, *J. Meteor. Soc. Japan*, **82**, 1187-1211.

Numaguti, A. (1999), Origin and recycling processes of precipitating water over the Eurasian continent: Experiments using an atmospheric general circulation model, *J. Geophys. Res.*, **104**, 1957-1972.

Okamura, O. and F. Kimura (2003), Behavior of GPS-derived precipitable water vapor in the mountain lee after the passage of a cold front, *Geophys. Res. Lett.*, **30**, 1746,

doi:10.1029/2003GL017572.

Oki, T., K. Musiake, H. Matsuyama, and K. Masuda (1995), Global atmospheric water balance and runoff from large river basins, *Hydrol. Process.*, **9**, 655-678.

Sato, T. (2005), The TianShan rain-shadow influence on the arid climate formation in northwestern China, *SOLA*, **1**, 13-16.

Sato, T., and F. Kimura (2005), Diurnal cycle of convective instability around the central mountains in Japan during the warm season, *J. Atmos. Sci.*, **62**, 1626-1636.

Sato, T., and F. Kimura (2006), Regional climate simulations to diagnose environmental changes in Mongolia, *Bull. Terrest. Env. Res. Center, Univ. of Tsukuba*, **7**, 59-69. (Available from http://www.suiri.tsukuba.ac.jp/bulletin/t7/t759.pdf)

Sato, T., F. Kimura, and A. Kitoh (2007), Projection of global warming onto regional precipitation over Mongolia using a regional climate model, *J. Hydrol.*, doi:10.1016/j.jhydrol.2006.07.023.

Sato, T., and F. Kimura (2007), Comparative study on the land-cover change and global warming impacts on regional climate in Northeast Asia, *Proceedings of the 19th Conference on Climate Variability and Change*, San Antonio, TX.

Sugita, M., J. Asanuma, M. Tsujimura, S. Mariko, M. Lu, F. Kimura, D. Azzaya, and Ts. Adyasuren (2007), An overview of the Rangelands Atmosphere-Hydrosphere-Biosphere Interaction Study Experiment in northeastern Asia (RAISE), *J. Hydrol.*, **333**, 3-20, doi:10.1016/j.jhydrol.2006.07.032.

Tremback, C. J. and R. Kessler (1985), A surface temperature and moisture parameterization for use in mesoscale numerical models, *Preprints, Seventh Conf. on Numerical Weather*

Prediction, Montreal, QC, Canada, Amer. Meteor. Soc., 355–358.

Trenberth, K. E. (1999), Atmospheric moisture recycling: Role of advection and local evaporation, *J. Climate*, **12**, 1368-1381.

Tsujimura, M., L. Sasaki, T. Yamanaka, A. Sugimoto, S.-G. Li, D. Matsushima, A. Kotani, and M. Saandar (2007), Vertical distribution of stable isotopic composition in atmospheric water vapor and subsurface water in grassland and forest sites, eastern Mongolia, *J. Hydrol.*, doi:10.1016/j.jhydrol.2006.07.025.

Ulbrich, U., and M. Christoph (1999), A shift of the NAO and increasing storm track activity over Europe due to anthropogenic greenhouse gas forcing, *Clim. Dyn.*, **15**, 551-559.

Walko, R. L., W. R. Cotton, M. P. Meyers, and J. Y. Harrington (1995), New RAMS cloud microphysics parameterization. Part 1: the single-moment scheme, *Atmos. Res.*, **38**, 29–62.

Watson, R. T., M. C. Zinyowera, and R. H. Moss (1998), *The regional impacts of climate change: an assessment of vulnerability*. *Special Report of IPCC Working Group II*, 517 pp. Cambridge University Press, Cambridge.

Xie, P., and P. A. Arkin (1997), Global Precipitation: A 17-year monthly analysis based on gauge observations, satellite estimates, and numerical model outputs, *Bull. Amer. Meteorol. Soc.*, **78**, 2539-2558.

Xue, Y. (1996), The impact of desertification in the Mongolian and the Inner Mongolian grassland on the regional climate, *J. Climate*, **9**, 2173-2189.

Yakir, D., and L. S. Sternberg (2000), The use of stable isotopes to study ecosystem gas exchange, *Oecologia*, **123**, 297-311.

1 Yamanaka, T., J. Shimada, and K. Miyaoka (2002), Footprint analysis using event-based isotope data
2 for identifying source 13 area of precipitated water, *J. Geophys. Res.*, **107(D22)**, 4624,
3 doi10.1029/2001JD001187.
4 Yamanaka, T., M. Tsujimura, D. Oyunbaatar, and G. Davaa (2007), Isotopic variation of precipitation
5 over eastern Mongolia and its implication for atmospheric water cycle, *J. Hydrol.*,
6 doi:10.1016/j.jhydrol.2006.07.022.
7 Yatagai, A., and T. Yasunari (1998), Variation of summer water vapor transport related to
8 precipitation over and around the arid region in the interior of the Eurasian continent, *J.*
9 *Meteor. Soc. Japan*, **76**, 799-815.
10 Yatagai, A. (2003), Evaluation of hydrological balance and its variability in arid and semi-arid
11 regions of Eurasia from ECMWF 15 year reanalysis, *Hydrol. Process.*, **17**, 2871-2884.
12 Yoshimura, K., T. Oki, N. Ohte, and S. Kanae (2003), A quantitative analysis of short-term ^{18}O
13 variability with a Rayleigh-type isotope circulation model, *J. Geophys. Res.*, **108(D20)**,
14 4647, doi10.1029/2003JD003477.
15 Yoshimura, K., T. Oki, N. Ohte, and S. Kanae (2004), Colored moisture analysis estimates of
16 variations in 1998 Asian monsoon water sources, *J. Meteor. Soc. Japan*, **82**, 1315-1329.
17 Yoshimura, K., S. Miyazaki, S. Kanae, and T. Oki (2006), Iso-MATSIRO, a land surface model that
18 incorporates stable water isotopes, *Glob. Planet. Change*, **51**, 90-107.
19

Figure captions

Figure 1: Atmospheric water budget around Mongolia (40-50^{o}N, 90-120^{o}E) evaluated using NCEP/NCAR reanalysis data during June, July, and August of 1979 - 2003. Arrows indicate the direction of water vapor transport. Unit is 1012 kg day^{-1}. Parentheses are standard deviations during 25-year analyzed period. PWV, P, C, and E in the figure indicate the area mean precipitable water vapor, precipitation, moisture convergence, and evapotranspiration, respectively. The CPC Merged Analysis of Precipitation (CMAP) is used for the precipitation. Evapotranspiration is calculated by E=P-C.

Figure 2: Observation sites (circles) and topography (m) around the study area. Broken line indicates the area where the ICM results are averaged (105-110^{o}E, 45-50^{o}N). Mongenmorit, 108.50^{o}E 48.20^{o}N; Ulaanbaatar, 106.87^{o}E 47.92^{o}N; Mandalgobi, 106.27^{o}E 45.75^{o}N; Choibalsan, 114.52^{o}E 48.07^{o}N; Underhaan, 110.67^{o}E 47.32^{o}N.

Figure 3: Time series of precipitable water vapor around the KBU site during June, July, and August of 2003. Dots are observed value by GPS. Thick and thin lines are obtained from the nearest gird points in regional climate model and NCEP/NCAR reanalysis data, respectively.

Figure 4: Scatter diagram of δ^{18}O in precipitation from observations and the ICM. Correlation coefficient for each station is shown in the bottom.

Figure 5: Time series of δ^{18}O in eastern Mongolia. Thin and thick lines indicate simulated δ^{18}O in precipitation and in water vapor, respectively, which are averaged over 105-110^{o}E, 45-50^{o}N. Circles with character and marks are corresponding to the δ^{18}O in collected precipitation at five sites. Stars indicate the observed vapor δ^{18}O by aircraft sounding in which

multiple-level data are averaged and shown as a daily mean by large stars while each observed value is shown by small stars. Broken line indicates the modeled vapor $\delta^{18}O$ around 114°E, 53.5°N.

Figure 6: Hovmoller diagram of the simulated $\delta^{18}O$ in water vapor over Mongolia along 80-130°E averaged at 41-50°N. Right panel shows the time series at KBU site using a nearest grid point value. Topography along the section is shown in the bottom.

Figure 7: Spatial distributions of (left) simulated $\delta^{18}O$ in water vapor and (right) hourly precipitation around Mongolia from 23rd June to 28th June 2003. Arrows indicate water vapor flux.

Figure 8: Time series of $\delta^{18}O$ tendency over eastern Mongolia as averaged over 105-110°E, 45-50°N during 23rd to 28th June (thick solid line). Dot line, broken line, and thin solid line indicate the amount of $\delta^{18}O$ change due to advection, precipitation, and evapotranspiration, respectively.

Figure 9: As in Figure 7 but for from 11th to 16th August 2003.

Figure 10: As in Figure 8 but for from 11th to 16th August 2003.

Figure 11: Definition of regions in the numerical domain of regional climate model. WSB, Western Siberia; ESB, Eastern Siberia; CTA, Central Asia; MON, Mongolia; NEA, Northeast Asia; TIB, Tibetan Plateau; ECA, East China; IDO, India and Indian Ocean; SEA, Southeast Asia; NPO, North Pacific Ocean; SPO, South Pacific Ocean. White boxes show the area averaged in Figure 12 and Figure 13.

Figure 12: Time series of water vapor sources over eastern Mongolia (105-110°E, 45-50°N) as estimated by the CMA. Colors indicate the amount of evapotranspiration from each region as defined in Figure 11. Colors below white line represent the moisture transported through

the lateral boundary of the model. Black area indicates the water vapor initially existed in the model domain. Integrated amount of all colored area coincides to the PWV. Right panel shows the June-July-August averaged water vapor sources.

Figure 13: As in Figure 12 except for Inner Mongolia, China (110-115^{o}E, 40-45^{o}N).

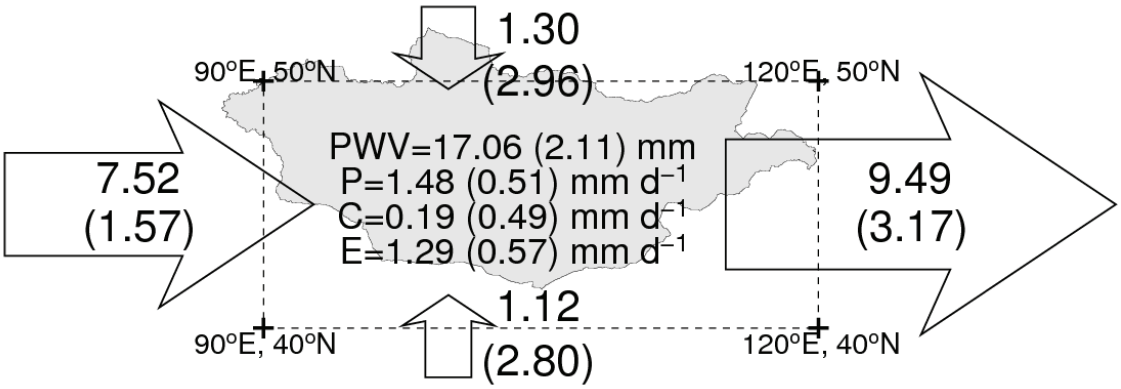

Figure 1: Atmospheric water budget around Mongolia (40-50°N, 90-120°E) evaluated using NCEP/NCAR reanalysis data during June, July, and August of 1979 - 2003. Arrows indicate the direction of water vapor transport. Unit is 10^{12} kg day^{-1}. Parentheses are standard deviations during 25-year analyzed period. PWV, P, C, and E in the figure indicate the area mean precipitable water vapor, precipitation, moisture convergence, and evapotranspiration, respectively. The CPC Merged Analysis of Precipitation (CMAP) is used for the precipitation. Evapotranspiration is calculated by E=P-C.

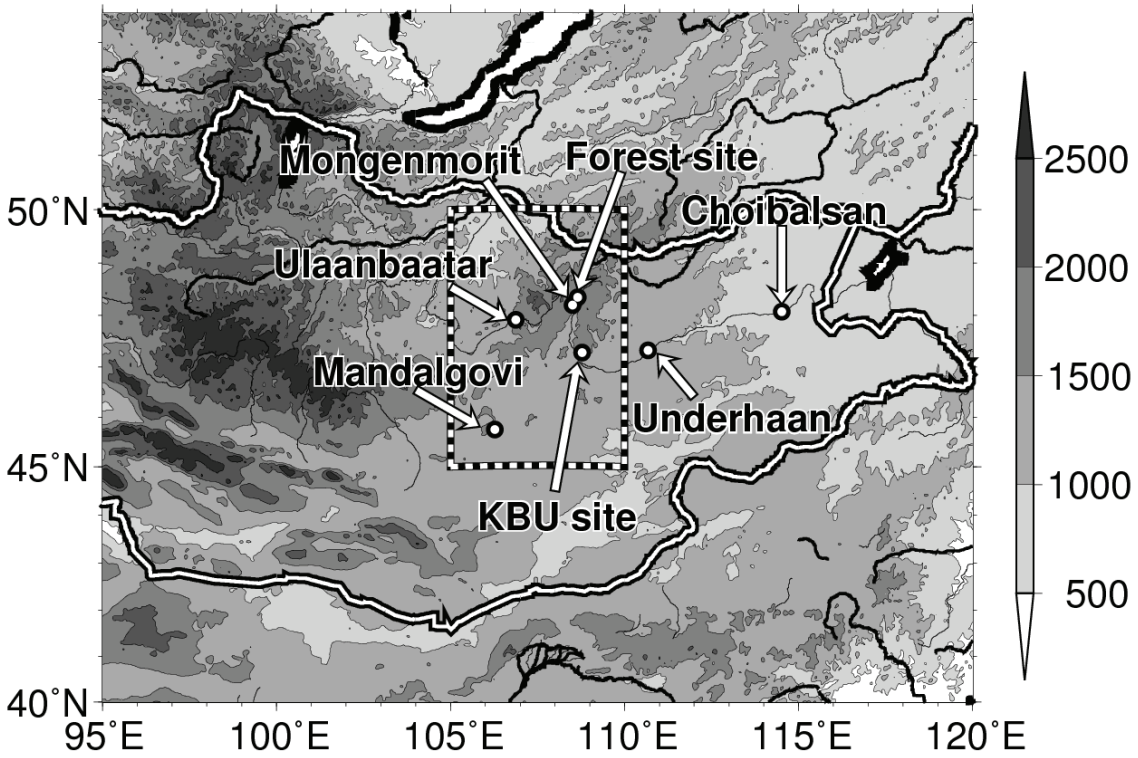

Figure 2: Observation sites (circles) and topography (m) around the study area. Broken line indicates the area where the ICM results are averaged (105-110^{o}E, 45-50^{o}N). Mongenmorit, 108.50^{o}E 48.20^{o}N; Ulaanbaatar, 106.87^{o}E 47.92^{o}N; Mandalgobi, 106.27^{o}E 45.75^{o}N; Choibalsan, 114.52^{o}E 48.07^{o}N; Underhaan, 110.67^{o}E 47.32^{o}N.

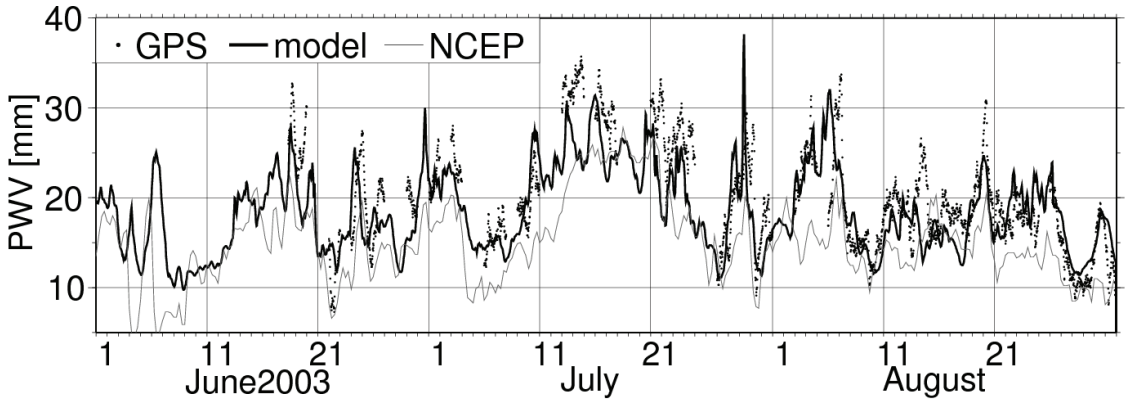

Figure 3: Time series of precipitable water vapor around the KBU site during June, July, and August of 2003. Dots are observed value by GPS. Thick and thin lines are obtained from the nearest gird points in regional climate model and NCEP/NCAR reanalysis data, respectively.

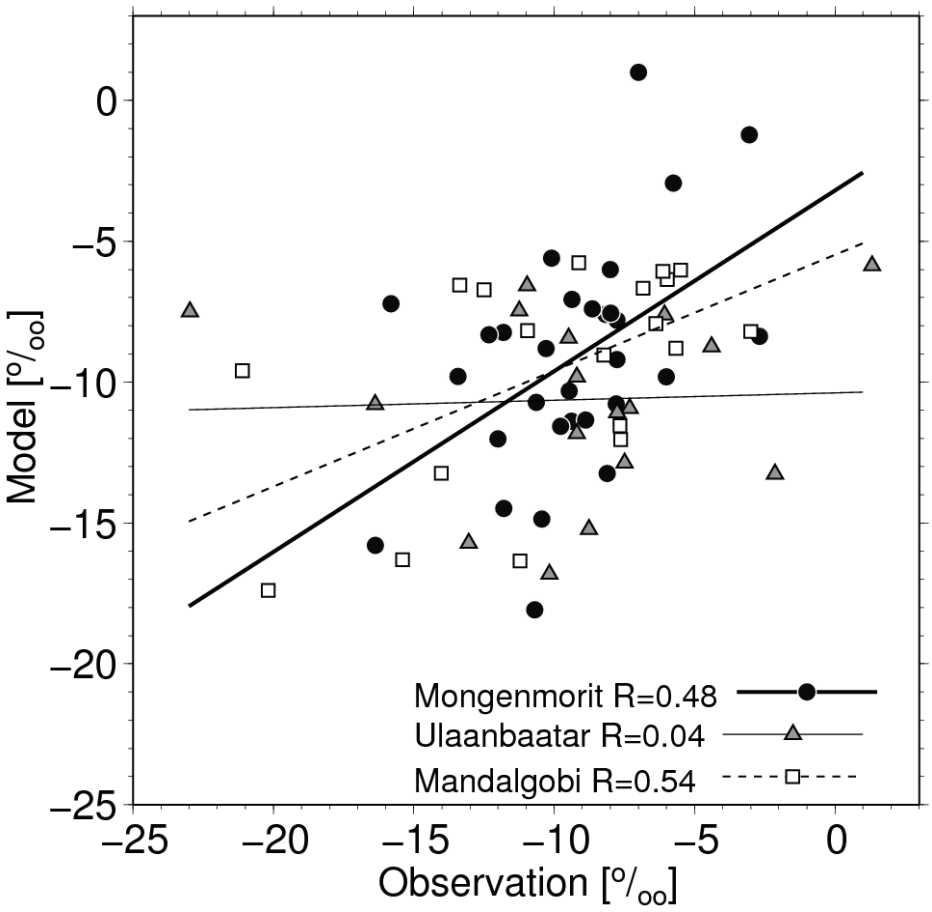

Figure 4: Scatter diagram of $\delta^{18}O$ in precipitation from observations and the ICM. Correlation coefficient for each station is shown in the bottom.

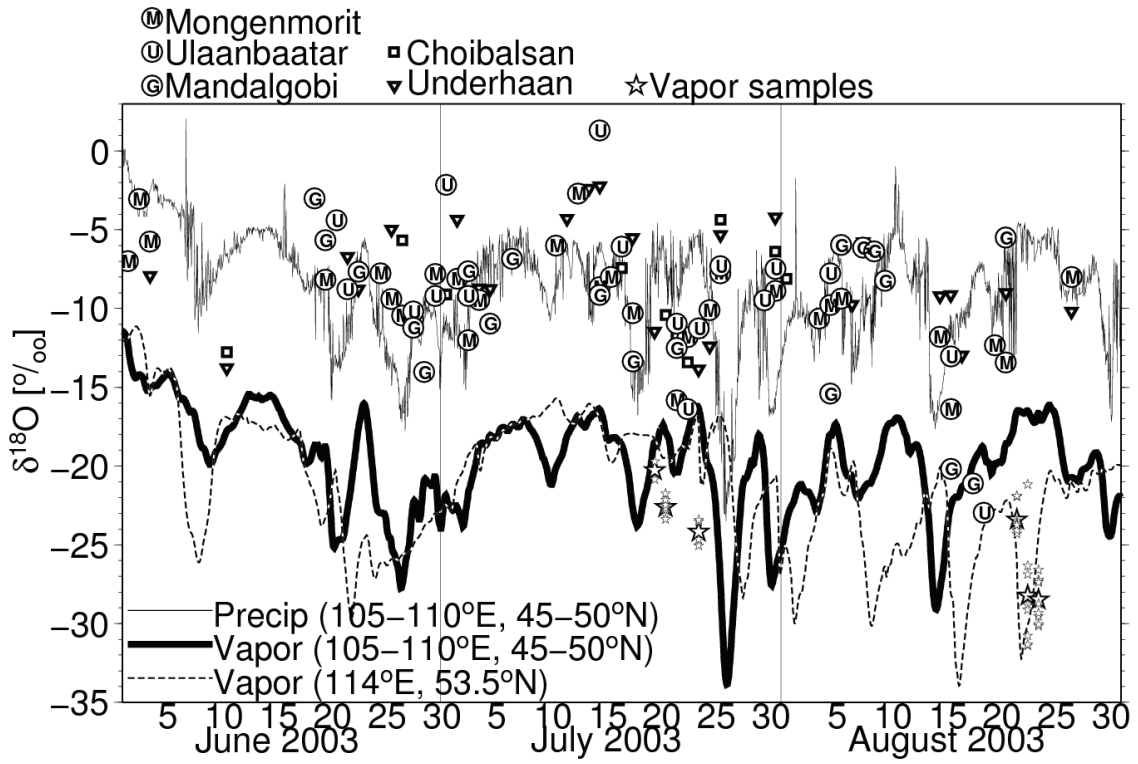

Figure 5: Time series of $\delta^{18}O$ in eastern Mongolia. Thin and thick lines indicate simulated $\delta^{18}O$ in precipitation and in water vapor, respectively, which are averaged over 105-110°E, 45-50°N. Circles with character and marks are corresponding to the $\delta^{18}O$ in collected precipitation at five sites. Stars indicate the observed vapor $\delta^{18}O$ by aircraft sounding in which multiple-level data are averaged and shown as a daily mean by large stars while each observed value is shown by small stars. Broken line indicates the modeled vapor $\delta^{18}O$ around 114°E, 53.5°N.

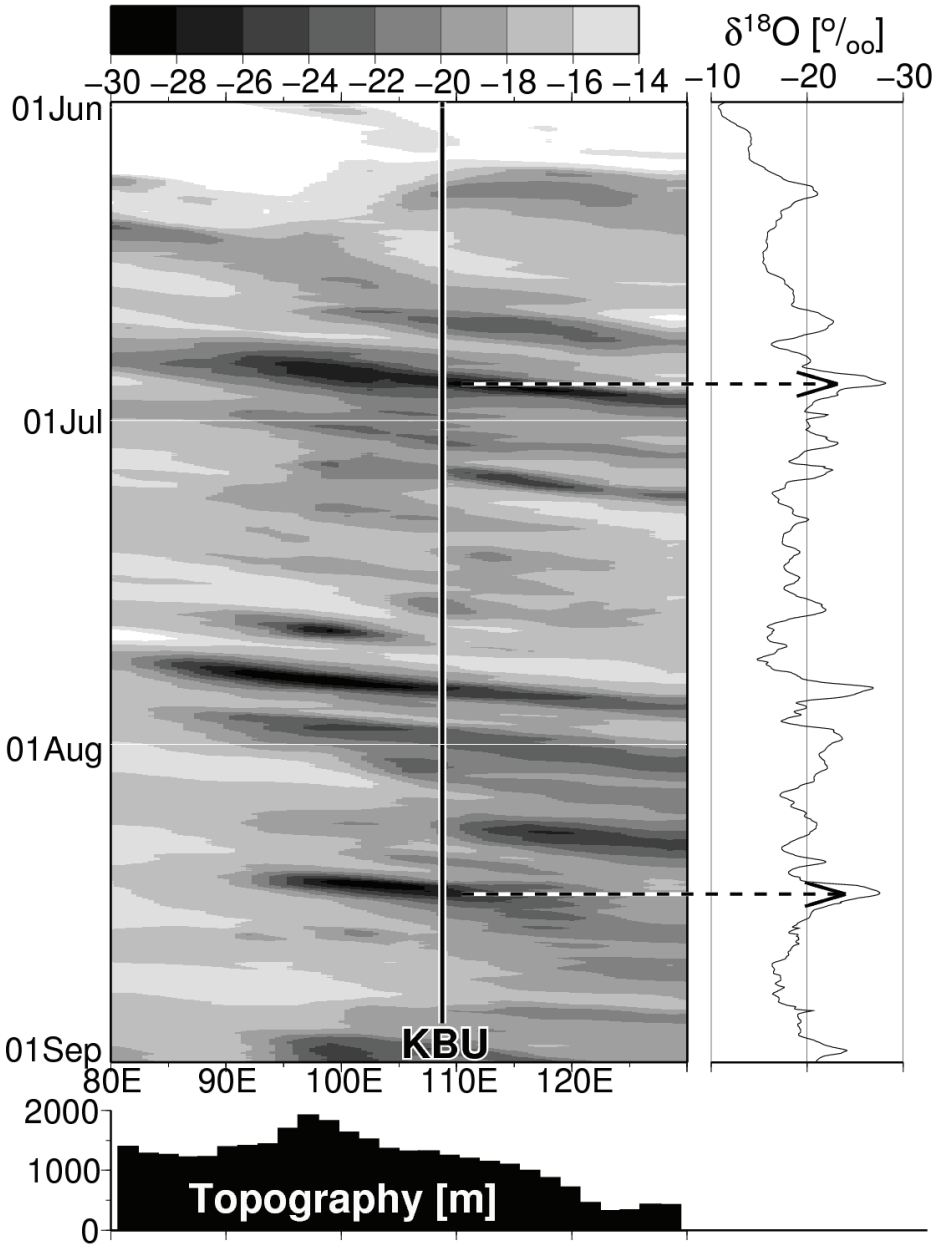

Figure 6: Hovmoller diagram of the simulated $\delta^{18}O$ in water vapor over Mongolia along 80-130^{o}E averaged at 41-50^{o}N. Right panel shows the time series at KBU site using a nearest grid point value. Topography along the section is shown in the bottom.

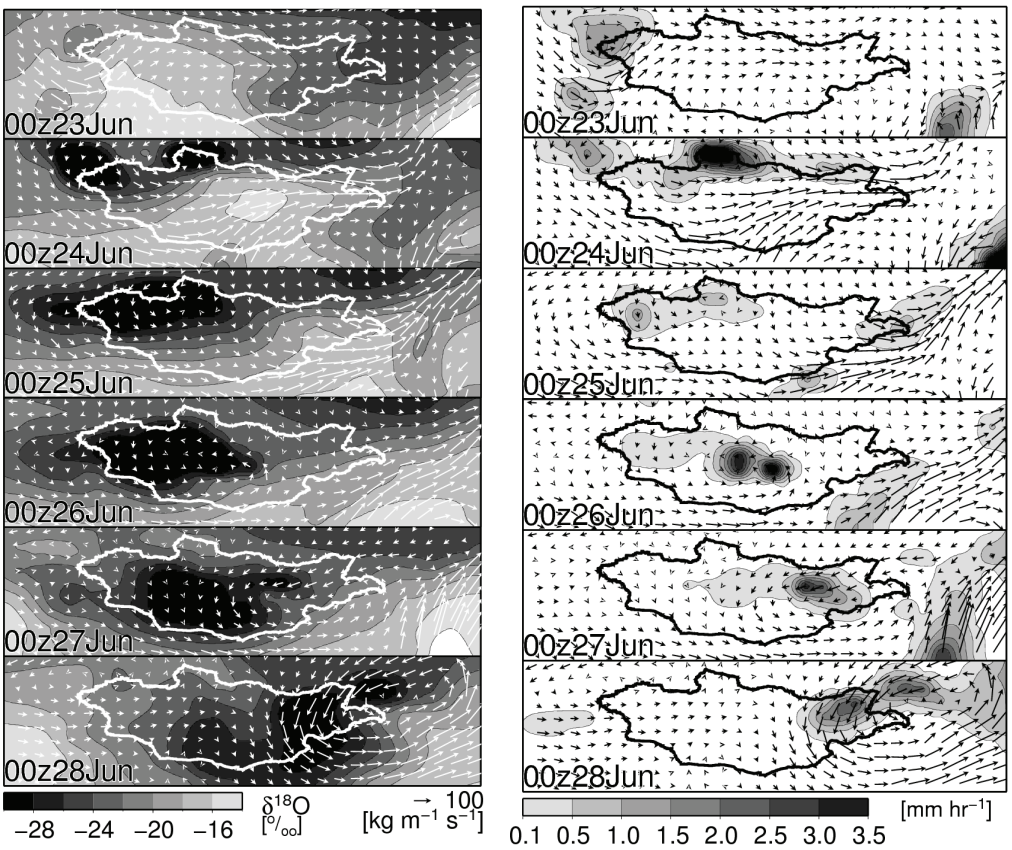

Figure 7: Spatial distributions of (left) simulated $\delta^{18}O$ in water vapor and (right) hourly precipitation around Mongolia from 23rd June to 28th June 2003. Arrows indicate water vapor flux.

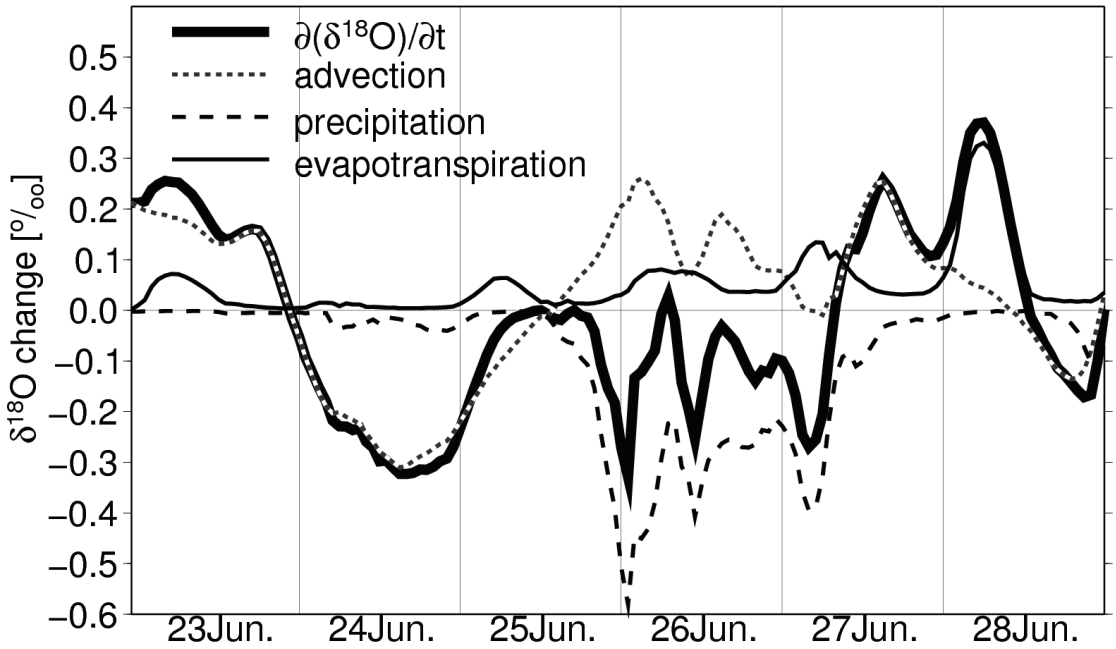

Figure 8: Time series of $\delta^{18}O$ tendency over eastern Mongolia as averaged over 105-110°E, 45-50°N during 23rd to 28th June (thick solid line). Dot line, broken line, and thin solid line indicate the amount of $\delta^{18}O$ change due to advection, precipitation, and evapotranspiration, respectively.

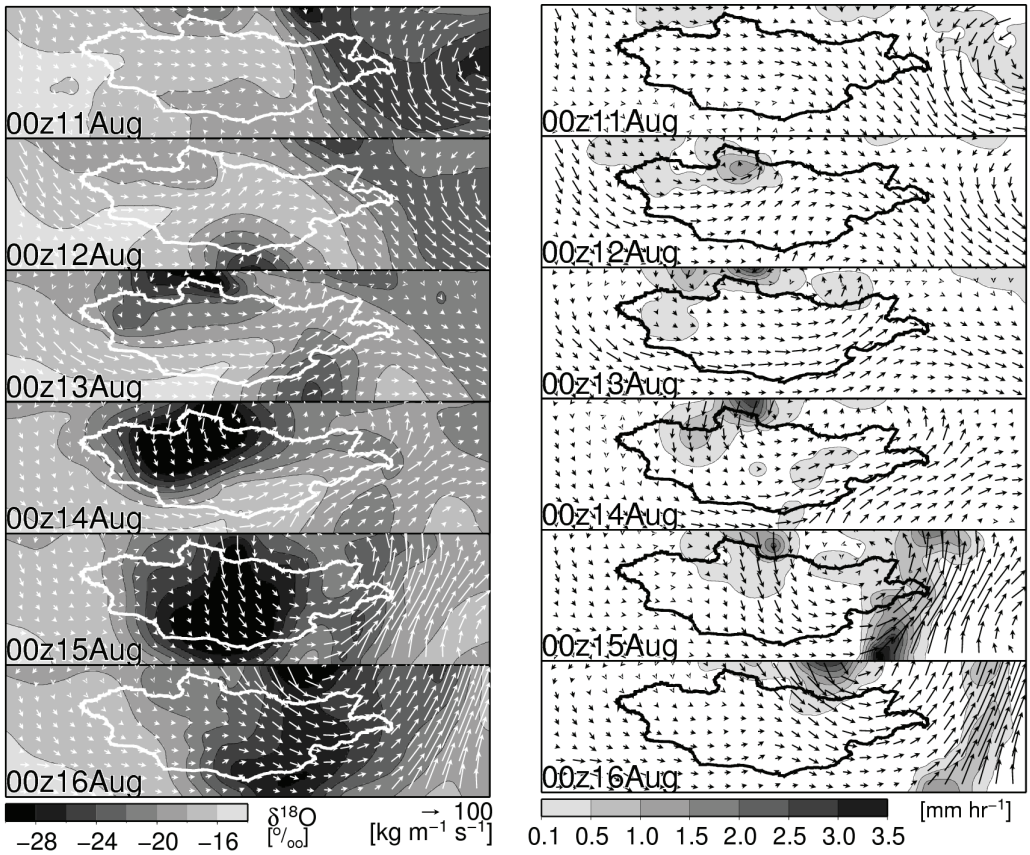

Figure 9: As in Figure 7 but for from 11th to 16th August 2003.

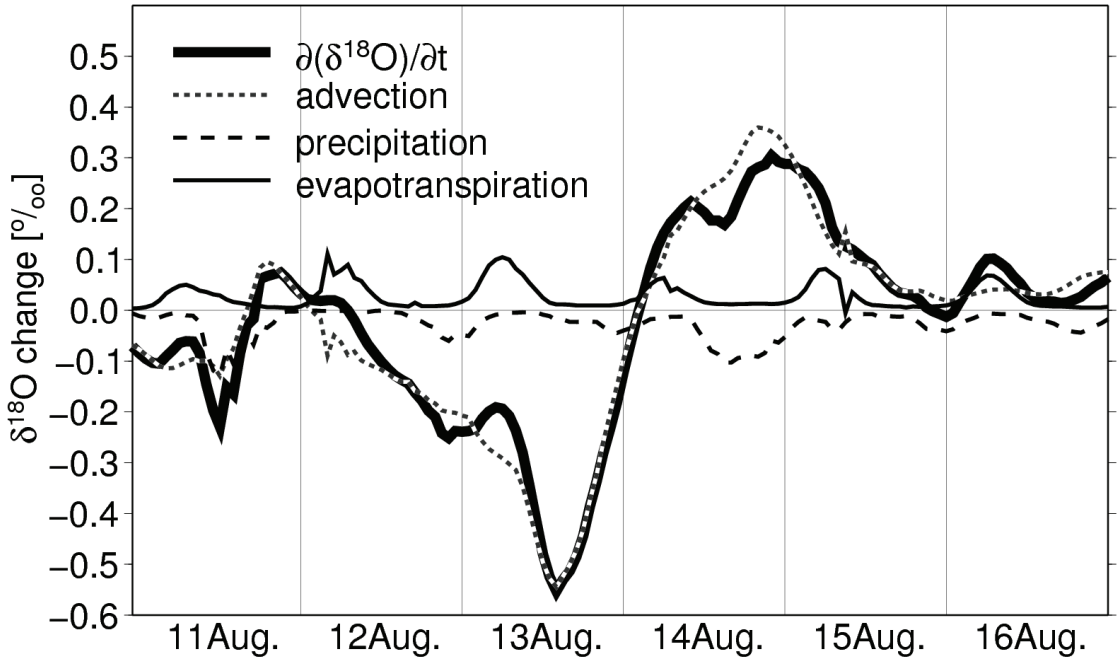

Figure 10: As in Figure 8 but for from 11th to 16th August 2003.

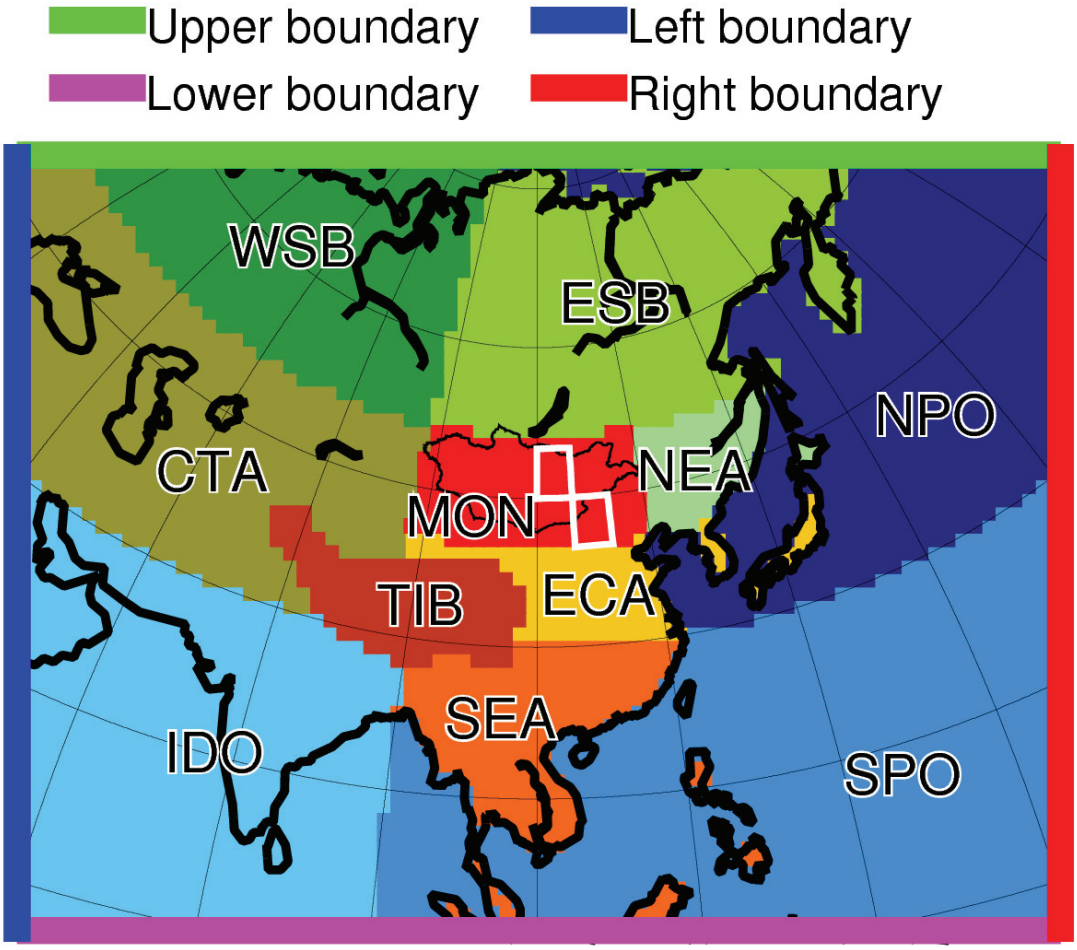

Figure 11: Definition of regions in the numerical domain of regional climate model. WSB, Western Siberia; ESB, Eastern Siberia; CTA, Central Asia; MON, Mongolia; NEA, Northeast Asia; TIB, Tibetan Plateau; ECA, East China; IDO, India and Indian Ocean; SEA, Southeast Asia; NPO, North Pacific Ocean; SPO, South Pacific Ocean. White boxes show the area averaged in Figure 12 and Figure 13.

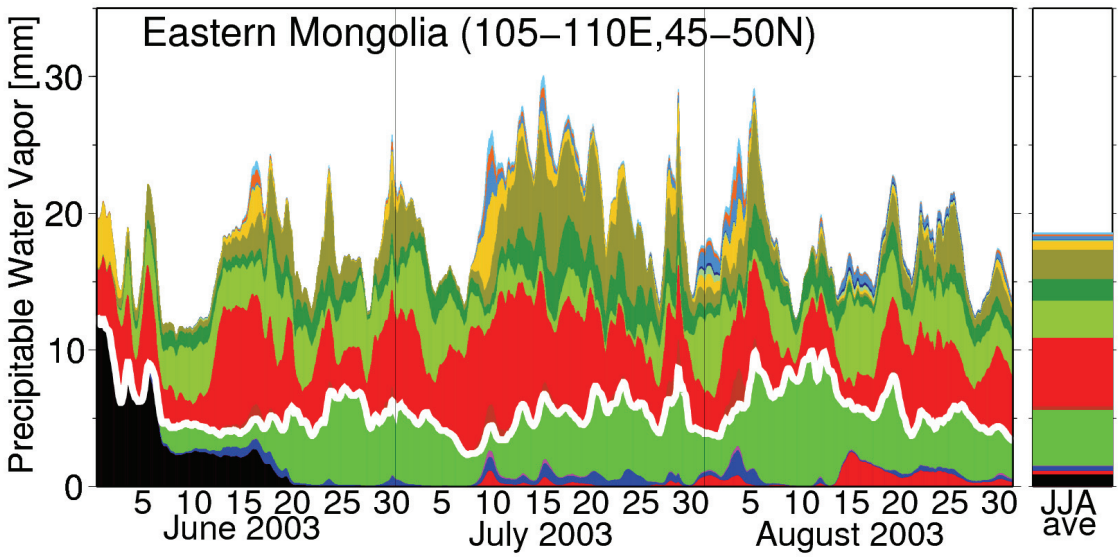

Figure 12: Time series of water vapor sources over eastern Mongolia (105-110°E, 45-50°N) as estimated by the CMA. Colors indicate the amount of evapotranspiration from each region as defined in Figure 11. Colors below white line represent the moisture transported through the lateral boundary of the model. Black area indicates the water vapor initially existed in the model domain. Integrated amount of all colored area coincides to the PWV. Right panel shows the June-July-August averaged water vapor sources.

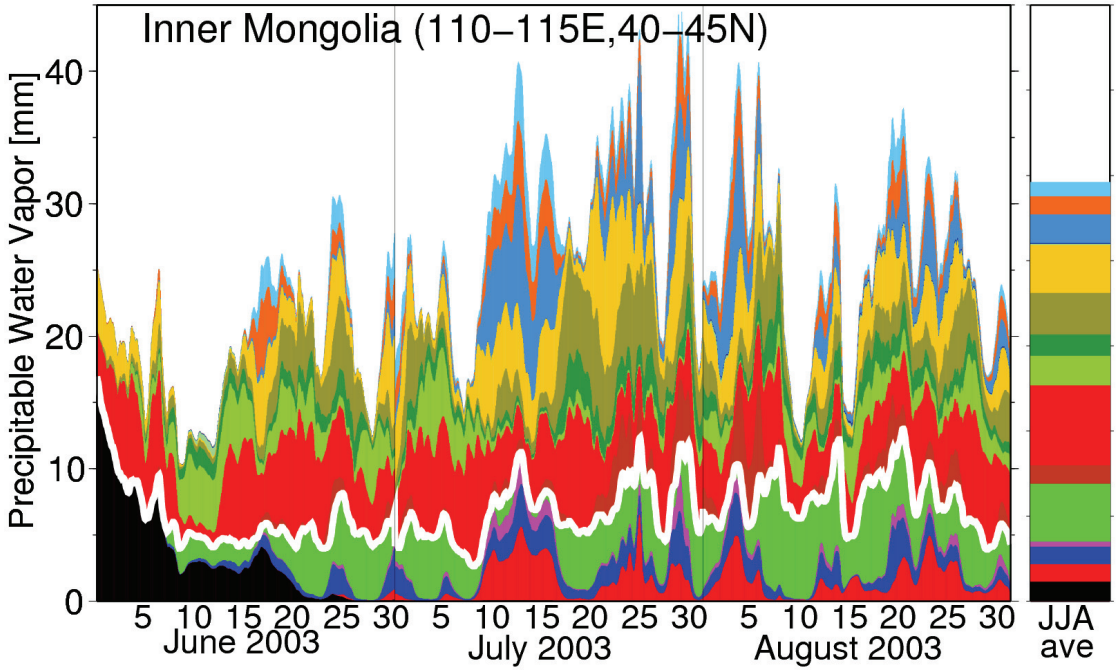

Figure 13: As in Figure 12 except for Inner Mongolia, China (110-115°E, 40-45°N).